Nanoscale

Accepted Manuscript

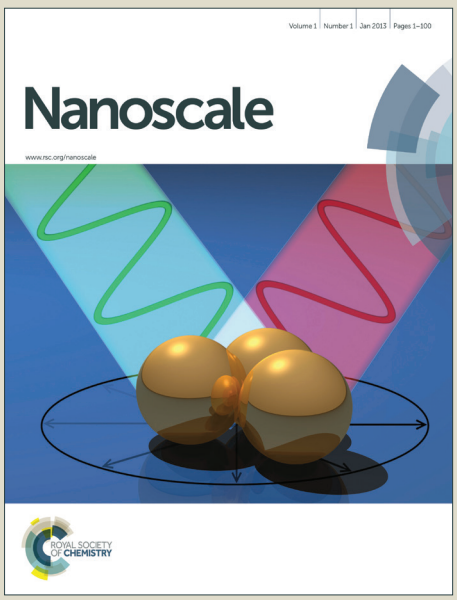

This is an *Accepted Manuscript*, which has been through the Royal Society of Chemistry peer review process and has been accepted for publication.

Accepted Manuscripts are published online shortly after acceptance, before technical editing, formatting and proof reading. Using this free service, authors can make their results available to the community, in citable form, before we publish the edited article. We will replace this *Accepted Manuscript* with the edited and formatted *Advance Article* as soon as it is available.

You can find more information about *Accepted Manuscripts* in the Information for Authors.

Please note that technical editing may introduce minor changes to the text and/or graphics, which may alter content. The journal's standard Terms & Conditions and the Ethical guidelines still apply. In no event shall the Royal Society of Chemistry be held responsible for any errors or omissions in this *Accepted Manuscript* or any consequences arising from the use of any information it contains.

ROYAL SOCIETY OF CHEMISTRY

www.rsc.org/nanoscale

Nanoscale

RSCPublishing

COMMUNICATION

Guided formation of sub-5 nm interstitial gaps between plasmonic nanodisks

Cite this: DOI: 10.1039/xoxxoooooox

Received ooth January 2012,
Accepted ooth January 2012

DOI: 10.1039/xoxxoooooox

www.rsc.org/

Jin Gyeong Son[a,b], Sang Woo Han[a,c], Jung-Sub Wi[b,*], Tae Geol Lee[b,*]

[a]*Department of Chemistry and KI for the NanoCentury, KAIST, Daejeon, 305-701, Korea*

[b]*Center for Nano-Bio Measurement, Korea Research Institute of Standards and Science, Daejeon, 305-340, Korea*

[c]*Center for Nanomaterilas and Chmeical Reactions, Institute for Basic Science (IBS), Daejeon, 305-701, Korea*

E-mail : jungsub.wi@kriss.re.kr, tglee@kriss.re.kr

To achieve a reliable formation of a surface-enhanced Raman scattering (SERS) sensor with evenly distributed hot spots on a wafer scale substrate, we propose a hybrid approach combining a physical nanolithography for preparing Au nanodisks and a chemical Au reduction for growing them. During the chemical growth, the interstitial distance between the nanodisks decreased from 60 nm to sub-5 nm. The resulting patterns of the nanogap-rich Au nanodisks successfully enhance the SERS signal, and its intensity map shows only a 5 % or less signal variation on the entire sample.

Introduction

Surface-enhanced Raman scattering (SERS) enables a highly-sensitive, non-destructive, and multiplexing molecular detection and has become a powerful tool to detect biomolecules, pharmaceuticals and environmental toxins.[1-3] Because surface-plasmon-induced electric-field enhancement is a key factor in the signal enhancement mechanism in SERS,[4,5] a reliable formation of a "hot spot", where the electromagnetic field enhanced by surface plasmon resonance can reach its highest value, is a prerequisite for practical uses of SERS. Hence, many technical approaches have been proposed for a reproducible SERS substrate with a high density of hot spots, one such approach being the lithography-based top-down fabrication.[6-10] Such electron-beam lithography (EBL) allows the production of a well-controlled plasmonic nanostructure with customized-size, -shape and -spacing.[11-13] However, the proximity effect originating from the scattering of incident electrons[14-16] makes it difficult to control the interstitial distance between neighboring nanostructures under 5 nm, a size-domain that is particularly attractive for the plasmonic hot-spots. Bottom-up approaches, on the other hand, such as self- or guided-assembly of nanoparticles, are easier to reduce the distance between the metallic nanoparticles down to 1 nm or less.[17,18] Considering the location, density, and signal enhancement factor of the hot spots, however, bottom-up methods are usually accompanied by loss of reproducibility.[19,20] There were a little attempts to utilizing the advantages of both approaches. Gopinath *et al.* tried to combine EBL with chemical growth, but randomly distributed small nanoparticles on aperiodic nanostructure reduce reproducibility because of different gap sizes. [21]

Here, we report a top-down and bottom-up combined method for the formation of sub-5 nm interstitial gaps in a wafer scale. In the proposed method, the array of Au nanodisks, which were patterned by nanoimprint lithography, functions as a preferential site for reducing Au ions in a solution mixture of hydrogen tetrachloroaurate(III) trihydrate ($HAuCl_4$ $3H_2O$)and hydroxylamine hydrochloride (NH_2OH HCl). Therefore, the interstitial distance between the Au nanodisks could be reduced during the Au reduction time from initially 60 nm to sub-5 nm. The evenly distributed sub-5 nm interstitial gaps, namely hot spots, on a whole sample were successfully verified by the analyses of molecular Raman signals and by numerical electromagnetic simulations.

Results and discussion

In order to prepare the array of sub-5 nm gaps, we used a top-down and bottom-up combined method, as illustrated in Fig. 1a. The top-down steps of the nanoimprint lithography (NIL) and Au evapor tion offer the distinct benefits of nanoscale resolution, reproducible patter

Nanoscale Accepted Manuscript

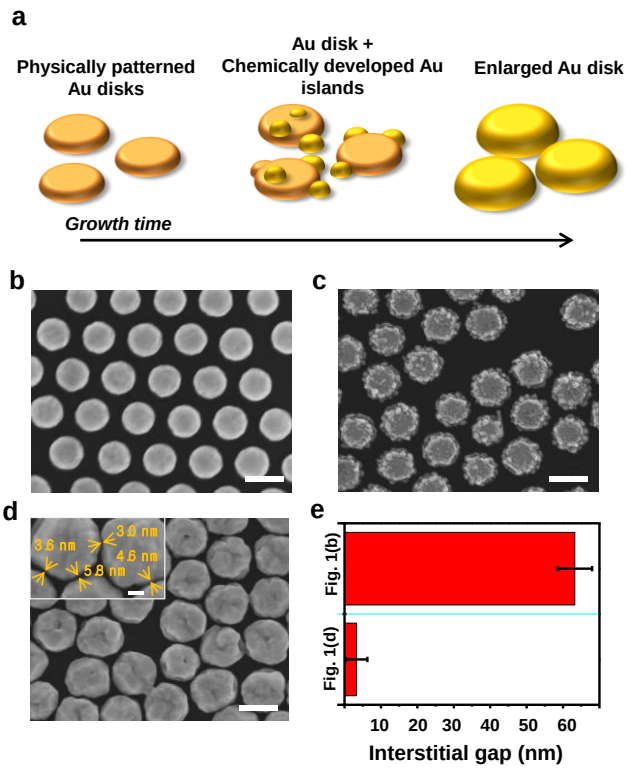

Fig. 1 (a) Illustration of the overall process used in this study: first, the arrays of uniform Au nanodisks are physically defined by nanoimprint lithography, and then the interstitial distances between the neighboring nanodisks are controlled by a solution-based chemical reduction of Au ions. SEM images of (b) physically patterned Au nanodisks, (c) Au nanodisks with chemically developed Au islands, and (d) enlarged Au nanodisks with interstitial nanogaps. The scale bars are 200 nm. (Inset) enlarged Au nanodisks interface gap size indications. The scale bar is 50 nm. (e) Statistics of the distance of the interstitial gaps analyzed with the protocol proposed for measuring the size of nanoparticles in SEM.[34]

-n generation, and high throughput.[22,23] In addition, by controlling the pattern size of the NIL mold and evaporated film thickness, the diameter and height of the Au nanodisk can be independently adjusted for plasmon-resonance with incident light.[24] In this study, the Au nanodisks which can interact with an excitation light of 633 nm wavelength (Fig. S1), were prepared on a full 4-inch-wafer by NIL which is practically difficult to achieve by EBL. Fig. 1b shows a typical SEM image of the lithographically patterned Au nanodisk. The mean diameter of the nanodisks and their interstitial distance is about 180 nm and 60 nm, respectively. Because our NIL mold was fabricated with self-assembled polystyrene beads,[10,25] partially closed packed nanodisks with vacant spaces that correspond to non-imprinted regions are commonly observed as shown in Fig. 1b-d. As part of the bottom-up process, chemical reduction of Au using NH_2OH/Au_3^+ mixtures was carried out for fine-tuning of the interstitial gaps between the Au nanodisks.[26] Because a heterogeneous nucleation is generally preferred over a homogeneous one,[27,28] the pre-patterned Au nanodisks work as energetically favorable sites for the Au reduction as follows: $3NH_2OH$ HCl (aq) + $4HAuCl_4$ (aq) + $3H_2O$ = $3HNO_2$ (aq) + $4Au^0$ (s) + 19 HCl (aq).[29] In the early stages of the Au reduction, therefore, several Au islands on the nanodisks were developed as shown in Fig. 1c. As the reduction progresses, the Au islands become large and interconnected (Fig. S2), and the surface of the nanodisk is flattened again to reduce the surface area, although it is relatively rough as compared to the initial Au surface. This surface morphology evolution of the Au disk is analogous to the coalescence process in a thin-film growth.[30,31] Because NH_2OH HCl is used as a reductant of $HAuCl_4$, high ratio of NH_2OH HCl to $HAuCl_4$ speeds up the reduction and narrows down the experimental window. In our experiments, the mixture ratio of 0.3 mM $HAuCl_4$ $3H_2O$ (99.9 %) 5 mL and 0.4 mM NH_2OH HCl (99 %) 5 mL was optimum. Moreover, the growth rate difference of Au on top of the nanodisks (~150-nm- increase in height for 20 min) and its sidewall surface (~60-nm-increase in diameter for 20 min) is also quite similar to the non-conformal thin-film growth on a non-planar surface.[32,33] Fig. 1d clearly demonstrates the evenly enlarged Au nanodisks, and consequently the narrowed interstitial gap between the nanodisks. During the reduction time of 20 min, the average diameter of the Au nanodisks increased from 180 nm to 237 nm, and the interstitial gap was successfully reduced to 3 nm with 2.9 nm of its standard deviation. The gap distances were evaluated by the statistical analysis protocol proposed for measuring the size of nanoparticles in SEM.[34]

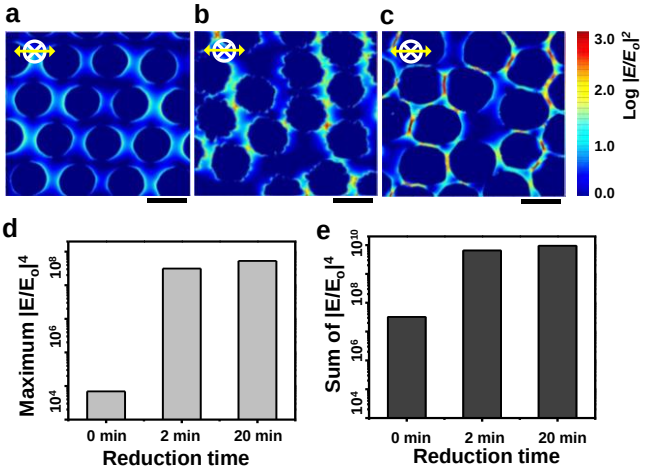

Fig. 2 Squared magnitude of the local field amplitude around (a) physically patterned Au nanodisks, (b) Au nanodisks with chemically developed Au islands, and (c) enlarged Au nanodisks with interstitial nanogaps. Incident light having a wavelength of 633 nm enters in the z-direction and is polarized in the x-direction, as indicated by the white and yellow arrows, respectively. All the scale bars are 200 nm. (d) The maximum and (e) the pixel-weighted sum of the $|E/E_0|^4$ values calculated from the entire area of the field contours in a–c.

To assess the effect of the prepared nanogap structure on SERS enhancement, a three dimensional finite-difference time-domain (FDTD) simulation was carried out using commercial software (Lumerical FDTD solution 8.9). For a proper simulation of the plasmonic structure, the SEM images of the nanodisks in Fig. 1b-d were imported and placed on the infinite Si substrate. The modeled structures were illuminated from the top by a linearly polarized plane wave with a wavelength of 633 nm, the wavelength employed for SERS experiments. Fig. S1 in supporting information also shows that the all modeled structures are activated most strongly at a wavelength between 600 nm and 700 nm. Because the electric field enhancement from a localized surface plasmon resonance is known to be the major mechanism for SERS,[4,5] two dimensional maps visualizing the enhanced electric fields of $|E/E_0|^2$, where E_0 and E are the amplitudes of the incident and enhanced electric fields, respectively, are shown in Fig. 2. The red-colored regions in the

Nanoscale Accepted Manuscript

This journal is © The Royal Society of Chemistry 2015

maps clearly show that the local electric field is strongly enhanced at the interstitial gaps between the nanodisks and that field enhancement increases with the Au reduction time. Quantitatively, the maximum and the pixel-weighted sum of $|E/E_0|^4$, which were calculated from each field map in Fig. 2a-c and displayed in Fig. 2d, e, increase respectively about 8000 times and 300 times by decreasing the gap distance from 60 nm to sub-5 nm.

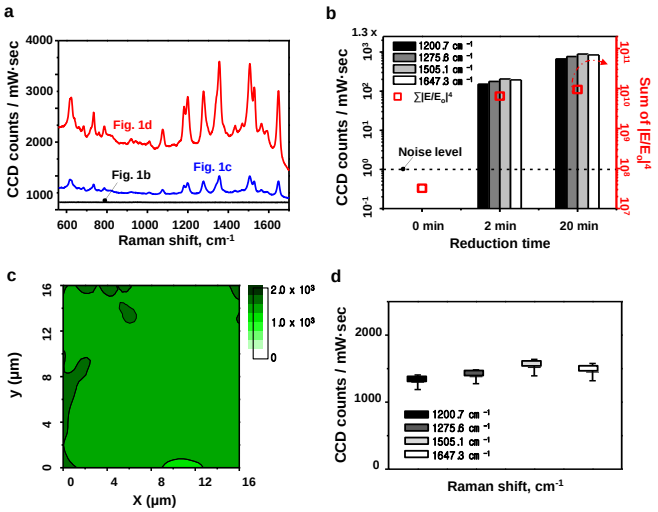

Fig. 3 (a) Representative SERS spectra of RITC molecules adsorbed on three different plasmonic nanostructures in Fig. 1a-c. All spectrum baselines are not corrected. (b) (Bar graph) The experimentally measured SERS intensities of major peaks in Fig. 3a and (red square) the calculated sum of $|E/E_0|^4$ values in Fig. 2e. (c) Two-dimensional intensity map of SERS intensity (1647.3 cm^{-1}) obtained from the 1-μM RITC treated Au nanodisks with sub-5 nm interstitial gaps. (d) SERS intensities of major peaks and their standard deviations analyzed from the entire area of the Fig. 3c.

The enhancement of the Raman signal depending on the interstitial distance between the Au nanodisks was experimentally demonstrated. Three samples of three different kinds of Au nanodisks in Fig. 1b-d were incubated in 10^{-6} M concentrated Rhodamine B isothiocynate (RITC) solution for 1 hour and rinsed with deionized water. Fig. 3a shows the representative Raman spectra of RITC molecules adsorbed on the three different nanostructures, and it is clear that the enhancement of SERS intensity increases with the Au reduction time. For a comparison of the simulated and experimental results, Raman intensities of several major peaks in Fig. 3a were plotted in Fig. 3b with the sum of $|E/E_0|^4$ values in Fig. 2e which are known to be proportional to the average intensities of the SERS signal.[35] If we consider the detection limit (three times of noise level) of our experiments, there should be a minimum of two orders of magnitude difference between the Raman intensities from the two samples of the initially patterned nanodisks and the final enlarged nanodisks. Therefore, these experimental results align reasonably well with the 300-fold-difference in the calculated sum values of $|E/E_0|^4$. The experimental value for enhancement factor (EF) was estimated to be about 1.5×10^5 (Fig. S3 and related text). Because the estimated diameter of the laser beam is about 858 nm and the beam size is correlates to about 10 nanodisks and their neighboring nanogaps, the experimentally assessed EF is its area-averaged value. The EF of our SERS substrate is rather low compared to the EF values reported in many previous studies including the substrate fabricated by nanosphere lithography. However, the study on the site distribution of SERS enhancement from Ag thin films on self-assembled nanospheres shows that the hottest sites (EF > 10^9) account for only 0.006% of the total.[36] The main advantage of our SERS substrate is its reliable performance based on evenly distributed hot spots as demonstrated below.

Finally, a two dimensional distribution of the Raman signal (1647.3 cm^{-1}) was mapped in Fig. 3c in order to verify the uniformity of our SERS substrate, the array of Au nanodisks with the interstitial nanogaps. The overall appearance of the SERS map in Fig. 3c shows the homogeneously enhanced Raman signal from the entire area, and the statistics of the Raman intensities in Fig. 3d shows only about 5 % of standard deviation. Zheng *et al*. evaluated a signal variation of the commercially available Klarite SERS substrate showed a 45 % spot to spot variation.[37] So far as we know, the most reproducible SERS substrate was a silver nanocluster made from copolymer micelles which showed around a 5 % signal variation.[38] Compared to the signals observed in previous reports and from commercial SERS substrate, the physically patterned and chemically enlarged Au disks have good SERS signal reproducibility for a large area. Moreover, the almost identical SERS intensities in Fig. 3b and d were actually obtained from two different samples fabricated from two different batches but are almost identical, which suggests batch-to-batch reproducibility.

Conclusions

We have presented a reliable and straightforward method for fabricating SERS substrates by combining top-down and bottom-up approaches. From the physical process, the overall shapes and dimensions of the Au nanodisks are defined by nanoimprint lithography and thin film deposition, and the interstitial distances between the nanodisks are controlled by the chemical process of Au reduction. The proposed method allowed us to form the array of Au nanodisks with sub-5 nm gaps, and concomitantly to enhance SERS activities which were confirmed by SERS experiments and numerical simulation. Because both the imprint-based nanopatterning and Au-reduction-chemistry-based pattern modifying can be scaled up to a wafer scale, and the presented results demonstrate a highly sensitive and spatially uniform molecular detection, we expect that our nanogap-controlled Au nanodisk array can be used as a practical SERS substrate.

Experimental section

Preparation of the array of Au nanodisks with sub-5 nm gap

Fig. 1a outlines the overall process used in this study. First, for the formation of the Au nanodisks, the spin-coated PMMA (mr-I PMMA, Microresist technology) / PMGI (PMGI SF3, Microchem) bilayer on a Si wafer was subjected to thermal nanoimprinting at 200 ^oC under a pressure of 30 bar for 5 min. After nanoimprinting, the residual PMMA layer was etched by O_2 plasma, and the sample was immersed in a commercial wet chemical developer (AZ MIF300, AZ electronic materials) for 3 s to form an undercut profile in the PMGI resist. Next, a 3 nm Ti adhesion layer followed by a 50 nm Au layer was deposited using thermal evaporation at a pressure of 2.0 x 10^{-6} Torr. After removal of the spin-coated polymers by AZ MIF 300 and rigorous sample cleaning by ethanol and water, the arrays of Au nanodisks were immersed for 2 and 20 min in mixtures of 0.3 mM $HAuCl_4$ $3H_2O$ (99.9 %) 5 mL and 0.4 mM NH_2OH (99 %) 5 mL. Then, the enlarged Au nanodisks were cleaned with deionized water (DW), and dried with nitrogen gas. Finally, the samples were

Nanoscale Accepted Manuscript

exposed to UV-ozone was adopted to remove possible contamination for 1 hr.

Instrumentation and characterization

For SERS measurements, the samples of the Au nanodisks were immersed in a RITC aqueous solution with a concentration of 10^{-6} M for 1 hr, and rinsed thoroughly with deionized water to remove non-specifically bound R6B molecules, and then dried with nitrogen gas. UV/O_3 exposure was performed using a commercial ozone cleaning system (PSD-UV, Novascan Technologies, Ames, IA, USA). The SERS measurements were performed using a laboratory-made micro-Raman system based on a 633 nm diode laser and a 50x objective lens with a thermoelectrically cooled CCD detector (iDUS 401, ANDOR). The laser power was 0.25 mW after passing through the lens and the focused spot size was estimated to be as 1.4 μm (≈ 1.22 λ/NA, with NA = numerical aperture = 0.55). The SERS spectra from a single point were obtained from with 3 s integration time. Sample surfaces were also mapped over 16 μm wide square frames with a unit pixel mesh of 1 μm × 1 μm and an accumulation time of 10 s $pixel^{-1}$.

Acknowledgements

This work was supported by the National Research Foundation of Korea (NRF) grant funded by the Korea government (MSIP) (No. 2010-0029149), the Bio-Signal Analysis Technology Innovation Program (NRF-2006-2005074), the Pioneer Research Center Program (NRF-2012-0009541), and Global Frontier Project (H-GUARD_2013M3A6B2078962) of MSIP/NRF.

References

1. J. N. Anker, W. P. Hall, O. Lyandres, N. C. Shah, J. Zhao, R. P. Van Duyne, *Nat. Mater.* 2008, **7**, 442–453.
2. C. Z. Zavaleta, B. R. Smitha, I. Waltonb, W. Doeringb, G. Davisb, B. Shojaeib, M. J. Natanb, S. S. Gambhir, *PNAS*, 2009, **106**, 13511-13516
3. J. F. Li, Y. F. Huang, Y. Ding, Z. L. Yang, S. B. Li, X. S. Zhou, F. R. Fan, W. Zhang, Z. Y. Zhou, D. Y. Wu, *Nature* 2010, **464**, 392–395.
4. S. J. Lee, Z. Guan, H. Xu, M. Moskovits, *J. Phys. Chem. C* 2007, **111**, 17985-17988
5. H. Y. Wu, C. J. Choi, B.T. Cunningham, *Small*, 2012, **8**, 2878-2885
6. A. L. Koh, A. I. Fernandez-Dominguez, D. W. McComb, S. A. Maier, J. K. W. Yang, *Nano Lett.* 2011, **11**,1323-1330
7. R. Stosch, F. Yaghobian, T. Weimann, R. J. C. Brown, M. J. T. Milton, B. Guttler, *Nanotechnology*. 2011, **22**, 105303
8. F. S. Ou, M. Hu, I. Naumov, A. Kim, W. Wu, A. M. Bratkovsky, X. Li, R. S. Williams, J. Li, *Nano Lett.* 2011, **11**, 2538-2542
9. A. W. Clark, J. M. Cooper, *Small*, 2011, **7**, 119-125
10. J. S. Wi, E. S. Barnard, R. J. Wilson, M. Zhang, M. Tang, M. L. Brongersma, S. X. Wang. *ACS nano*, 2011, **5**, 6499-6457.
11. A. Nahla, H. Abu, J.M.Oran, J. S. Michael, *ACS nano*, 2008, **2**, 377-385
12. T. Jesse, P. Prathamesh, M. E. Pierre, E. M. Richard, B. C. Stephen, *Nano Letters*, 2010, **10**, 2749-2754
13. D. Huigao, H. Hailong, K. Karthik, S. Zexiang, K. W. Y. Joel, *ACS nano*, 2011, **9**, 7593-7600
14. N. Samoto, R. Shimizu, *J. Appl. Phys.* 1983, **54**, 3855-3859
15. A. N. Broers, A. C. F. Hoole, I. M. Ryan, *Microelectronic Engineering*, 1996, **32**, 131-142
16. J. S. Wi, H. S. Lee, K. Lim, S. W. Nam, H. M. Kim, S. Y. Park, J. J. Lee, C. D. Hong, S. Jin, K. B. Kim, *Small*, 2008, **4**, 2118-2122
17. D. K. Lim, K. S. Jeon, H. M. Kim, J. M. Nam, Y. D. Suh, *Nature materials*, 2010, **9**, 60-67
18. D. K. Lim, K. S. Jeon, J. H. Hwang, H. Kim, S. Kwon, Y. D. Suh, J. M. Nam, *Nature Nanotechnology*, 2011, **6**, 452-460
19. M. J. Mulvihill, X. Y. Ling, J. Henzie, P. Yang, *J. Am. Chem. Soc*, 2010, **132**, 268-274
20. Z. Zhu, H. Meng, W. Liu, X. Liu, J. Gong, X. Qiu, L. Jiang, D. Wang, Z. Tang, *Angew. Chem*. 2011, **123**, 1631 –1634
21. A. Gopinath, S. V. Boriskina, W. R. Premasiri, L. Ziegler, B. M. Reinhard, L. D. Negro, *Nano Letters*, 2009, **9**, 3922-3929
22. S. Y. Chou, P. R. Krauss, P. J. Renstrom, *J. Vac. Sci. Technol*, 1996, **B 14**, 4129–4133
23. L. J. Guo, *Adv. Mater*. 2007, **19**, 495–513
24. B. D. Lucas, J-S Kim, C. Chin, L. J. Guo, *Adv. Mater*. 2008, **20**, 1129-1134
25. J. S. Wi, S. Sengupta, R.J. Wilson, M. Zhang, M. Tangm S. X. Wang, *Small*, 2011, **7**, 3176-3280
26. Y. P. Kim, T. G. Lee, *Anal chem*. 2012, **84**, 4784-4788
27. V. K. Lamer, R. H. DInegar, *J. Am. Chem. Soc*, 1950, **72**, 4847-4854
28. A. E. Neilsen, Kinetics of Precipitation. Pergamon, 1964, Oxford
29. L. D. Burke, P. F. Nugent, *Gold bulletin*, 1997, **30(2)**, 43-53
30. J. A. Venables, G. D. T. Spiller, M. Hanbucken, *Rep. Prog. Phys*. 1984, **47**, 399-459
31. M. Oring, *The Materials Science of Thin Films*. Elizabeth E. T. ACADEMIC PRESS, San Diego, 2001, 195-198
32. J. D. Plummer, M. D. Deal, P. B. Griffin, Silicon VLSI Technology, Prentice Hall, Upper Saddle River, NJ, 2000, 509-605
33. H. S. Baxamusa, S.G.Im, K.K.Gleason, *Phys. Chem. Chem. Phys*., 2009, **11**, 5227-5240
34. A. E. Vladár, B. Ming, NIST - NCL Joint Assay Protocol, PCC-15 ver. 1.0 1-20, 2011
35. F. J. Garcı´a-Vidal, J. B. Pendry, *Phys. Rev. Lett.* 1996, **77**, 1163-1166
36. Y. Fang, N-K Seong, D.D.Dlott, *Science*, 2008, **321**, 388-340
37. Y. Zheng, T. Thai, P. Reineck, L. Qiu, Y. Guo, U. Bach, *Adv. Funct. Mater*. 2013, **23**, 1519-1526
38. W. J. Cho, Y. Kim, J. K. Kim, *ACS nano*, 2012, **6**, 249-255

Nanoscale Accepted Manuscript

 This journal is © The Royal Society of Chemistry 2015